EPJ Web of Conferences **60**, 19007 (2013)
DOI: 10.1051/epjconf/20136019007

Electroweak boson production at LHCb

Ronan Wallace[1,a] on behalf of the LHCb Collaboration.

[1] *University College Dublin,*
School of Physics,
Science Centre North,
Belfield, Dublin 4,
Ireland.

Abstract. Measurements of W and Z boson production provide important tests of the Standard Model as well as being inputs for determining the parton density functions of the proton. W and Z production cross-sections, and their ratios, have been measured using the LHCb detector and are reported here. Datasets of up to 1 fb^{-1} at $\sqrt{s}$ = 7 TeV are used.

1 Introduction

Measurements of the W and Z production cross-sections and cross-section ratios test the Standard Model (SM) and can be used to constrain proton parton density functions (PDFs) where those are not well known. For a W or Z boson to be produced within LHCb's forward acceptance ($2 < \eta < 5$), a valence quark carrying a high fraction of the proton momentum must annihilate with a sea quark carrying a low momentum fraction. This corresponds to the high-x $\sim 10^{-1}$ and low-x $\sim 10^{-4}$ of the $\left(x, Q^2\right)$ kinematic region with $Q^2 \sim 10^4$ GeV^2, where x denotes momentum fraction and Q^2 momentum transfer. Thus PDFs can be constrained in two distinct regions. In this way LHCb complements the work of detectors with central pseudorapidity coverage.

While the cross-sections themselves are sensitive to PDFs, measuring the ratios of these cross-sections can highlight or largely cancel the PDF dependence. The lepton charge asymmetry[b] and the ratio of W^+ to W^- production are sensitive to the ratio of the up and down valence quark PDFs. The ratio of W production to Z production is almost independent of PDF uncertainty and is thus a precision test of the SM.

The 2011 data sample (1 fb^{-1} at $\sqrt{s}$ = 7 TeV) has been used to measure the $Z \to \tau\tau$ [1], $Z \to \mu\mu$ [2] and $Z \to ee$ [3] production cross-sections. The cross-sections have been measured differentially in the $Z \to \mu\mu$ and $Z \to ee$ channels as functions of rapidity and ϕ^{*}[c] [4] of the Z boson. The cross-section has also been measured differentially as a function of boson transverse momentum in the $Z \to \mu\mu$ channel.

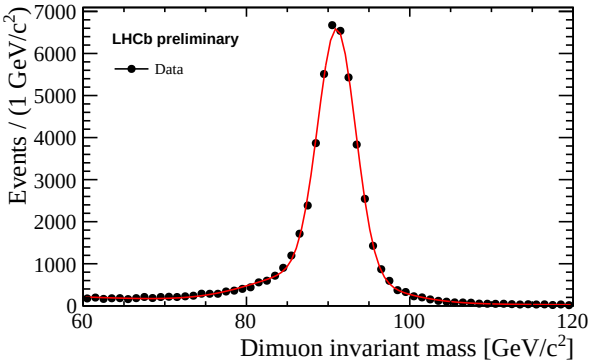

Figure 1. Di-muon invariant mass. The data are shown as points and they have been fitted with a double Gaussian.

The 2010 data sample (37 pb^{-1} at $\sqrt{s}$ = 7 TeV) has been used to measure W and Z cross-sections, the ratio of the W^+ to W^-, the lepton charge asymmetry and the ratio of W to Z production [5].

2 $Z \to \ell^+\ell^-$

In the muon and electron channels, Z events are selected by requiring two well reconstructed and oppositely charged leptons in the pseudorapidity range between 2.0 and 4.5 with transverse momentum $p_T > 20$ GeV/c. The invariant mass of the di-muon combination is required to be between 60 GeV/c^2 and 120 GeV/c^2. Figure 1 shows the di-muon invariant mass of the selected events. The reconstructed di-electron mass needs to be greater than 40 GeV/c^2. Figure 2 shows the di-electron mass of the selected events. The distribution falls off abruptly above the Z mass and is spread to lower masses. The reason for the large tail is bremsstrahlung; the energy of the electron is

[a] e-mail: ronan.wallace@cern.ch
[b] See section 4 for definition.
[c] $\phi^* = \frac{tan((\pi - |\Delta\phi|)/2)}{cosh(\Delta\eta/2)}$

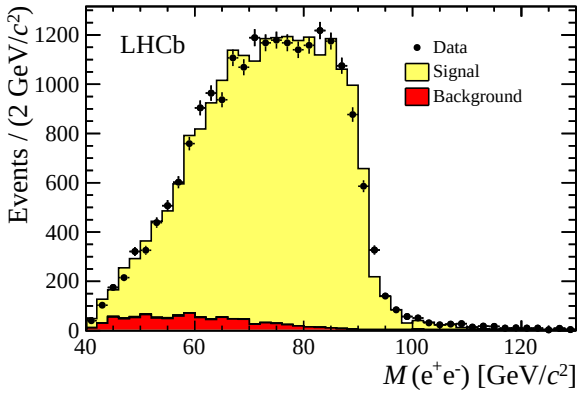

Figure 2. Di-electron invariant mass. The data are shown as points and the histograms show signal and background contributions.

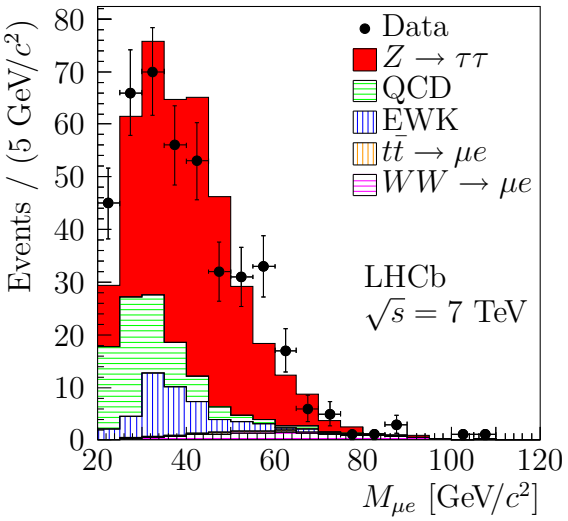

Figure 3. Reconstructed mass of muon-electron combination. The data are shown as points and and histograms show signal and background contributions.

measured from the tracks because the LHCb calorimeter saturates at high energies and cannot be used for this analysis. Z events which decay to tau-leptons are selected by requiring one $p_T > 20$ GeV/c electron or muon accompanied by an opposite sign electron, muon or charged hadron with $p_T > 5$ GeV/c. The invariant mass of the combination is required to be greater than 20 GeV/c^2. The analysis is thus broken down into five different streams $\tau_\mu\tau_\mu$, $\tau_\mu\tau_e$, $\tau_e\tau_\mu$, $\tau_\mu\tau_h$ and $\tau_e\tau_h$. Electrons are required to deposit 50 MeV in a pre-shower detector and leave large ($E/pc > 0.1$) and small ($E/pc < 0.05$) deposits in the electromagnetic and hadronic calorimeters respectively. Here E is the energy measured in the respective calorimeter and p the momentum reconstructed from the tracks. A number of further cuts are applied in the $Z \to \tau\tau$ selection to reject different types of backgrounds. Further details can be found in [1]. Shown in Figure 3 is the mass of the tau decay product candidates, in this case a muon and an electron.

The largest remaining backgrounds for all three decay channels of the Z are estimated using data driven methods. The contribution from semileptonic heavy flavour decays is estimated by exploiting the fact that the resulting muons are non-prompt and are accompanied by QCD activity. This is the largest background in the $Z \to \mu\mu$ channel. Same-sign events are used to quantify backgrounds in all three leptonic decays of the Z. π/K decay in flight and punch-through background for $Z \to \mu\mu$ is expected to contribute equally in same-sign and opposite-sign pairs as is the early showering of hadrons faking electrons, the dominant background in the $Z \to ee$ channel. The $Z \to \mu\mu$ and $Z \to ee$ selections are quite pure with purities of 99.7% and 95.5% respectively. QCD and electroweak (where a high p_T lepton comes from W and Z decay and the other from the underlying event) backgrounds are dominant in the $Z \to \tau\tau$ channel which again are estimated from same-sign data.

3 $W \to \mu\nu$

$W \to \mu\nu$ events are selected by requiring a well reconstructed muon with high transverse momentum $20 < p_T <$

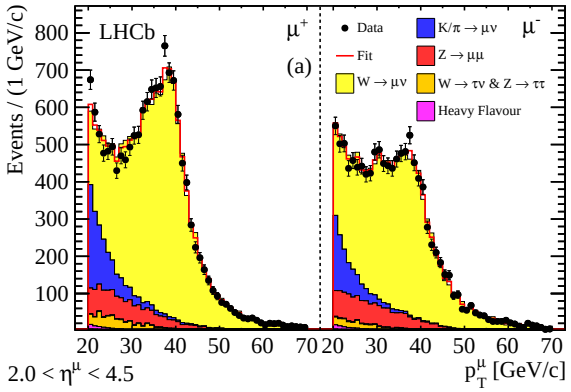

Figure 4. μ^+ (left) and μ^- (right) p_T spectra on the 2010 dataset. The black points show the data. The histograms show the various signal and background contributions.

70 GeV/c in the pseudorapidity range between 2.0 and 4.5. It is also required that no other opposite-sign muon with transverse momentum greater than 2 GeV/c is in the event. To suppress decays from long lived particles, the muon impact parameter is required to be less than 40 μm. QCD background is removed using isolation cuts.

To estimate purity, signal and background templates are fitted to the p_T distribution of the muons (see Figure 4). Signal and $Z \to \mu\mu$ templates are obtained from NNLO simulation. In each pseudorapidity bin the normalisation for signal floats while that for the $Z \to \mu\mu$ background is fixed from data. The background template for decay in flight of pions or kaons before the muon chambers is determined by weighting the transverse momentum distribution of charged hadrons with the momentum dependent probability that the hadron decays to a muon,

given by $Prob\,(p) = 1 - e^{-\alpha/p}$. The normalisation in each bin is free to vary. Other backgrounds include $W \to \tau\nu$, $Z \to \tau\tau$ (templates from simulation) and decays of B and D hadrons (template from data). These normalisations are fixed. Decay in flight and $Z \to \mu\mu$ backgrounds are the dominant contributions. The total purities for both W^+ and W^- are about 78%.

4 Results

Inclusive differential cross-sections of W and Z are calculated for leptons with $p_T > 20$ GeV/c and pseudorapidities between 2.0 and 4.5. In the case of the Z the di-lepton invariant mass must be between 60 and 120 GeV/c^2. Representative of the formulas being used is that for $Z \to \mu\mu$

$$\sigma\,(i) = \frac{\rho f_{FSR}\,(i)\, f_{MGR}\,(i)}{\mathcal{L}\mathcal{A}} \sum_k \frac{1}{\epsilon\left(\eta_k^{\mu^+}, \eta_k^{\mu^-}, PV_k\right)}$$

where the reconstruction efficiency ϵ depends on muon pseudorapidity and the number of primary vertices in the event. The prefactors account for the purity of the sample ρ, final state radiation f_{FSR}, bin migrations f_{MGR}, acceptance $\mathcal{A}$ and integrated luminosity $\mathcal{L}$. The total cross section is calculated by summing over bins i.

The reconstruction efficiency ϵ mentioned above is determined from data using a tag-and-probe method. It can be broken down into three separate components; an efficiency for the event to be triggered, an efficiency for both muons to be identified as so, and an efficiency for muon track reconstruction. No evidence of charge or magnet polarity bias nor dependence on p, p_T nor ϕ is observed. Uncertainties on the efficiencies are statistical and systematic, the latter being deduced from the observed differences between efficiencies evaluated with true and reconstructed information in simulation.

The dominant systematic uncertainties in the $Z \to \mu\mu$ channel are the muon tracking efficiencies and reconstruction effects which manifest when the analysis is performed with different magnet polarities. These are each $\sim$ 1.1%. Limiting the measurement in the electron channel are electron tracking efficiencies and kinematic efficiencies at the level of $\sim$ 1.6% and $\sim$ 1.4% respectively. In the $\tau_\mu\tau_\mu$ stream the background uncertainty is dominant at $\sim$ 10%. In the other leptonic final states $\tau_\mu\tau_e$ or $\tau_e\tau_\mu$, the reconstruction efficiencies dominate at $\sim$ 5%. For final states containing hadrons the selection efficiency dominates at $\sim$ 4.6%.

The dominant systematic uncertainties for the $W \to \mu\nu$ measurement are the muon reconstruction and selection efficiencies which both contribute about $\sim$ 2%. The signal purity and template fits both contribute $\sim$ 1%.

Results for Z cross-sections measured using the 2011 dataset are compared to next-to-next-to-leading-order (NNLO) predictions made by FEWZ [6] with MSTW08 PDFs [7]. These comparisons can be seen in Figure 5. The simulation and data are in excellent agreement. The measured cross-sections are quoted below with the first uncertainty being statistical, the second systematic and the third due to luminosity.

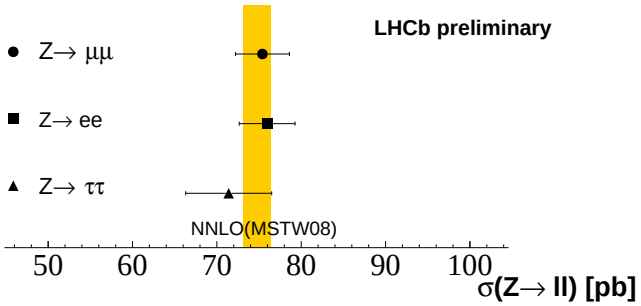

Figure 5. Cross-sections in common fiducial (points) for different leptonic decays of the Z compared to FEWZ NNLO predictions with MSTW08 PDF set (band). The width of the band corresponds to PDF and scale uncertainties.

$$\sigma\,(Z \to \mu\mu) = 75.4 \pm 0.3 \pm 1.6 \pm 2.6 \text{ pb}$$
$$\sigma\,(Z \to ee) = 76.0 \pm 0.8 \pm 2.0 \pm 2.6 \text{ pb}$$
$$\sigma\,(Z \to \tau\tau) = 71.4 \pm 3.5 \pm 2.8 \pm 2.5 \text{ pb}$$

The ratios $\sigma\,(Z \to \tau\tau)\,/\sigma\,(Z \to \mu\mu) = 0.93 \pm 0.09$, $\sigma\,(Z \to ee)\,/\sigma\,(Z \to \mu\mu) = 0.99 \pm 0.05$ show universality of the Z to lepton couplings. The differential cross-section as a function of the Z boson ϕ^* is shown in Figure 6. The purely perturbative prediction (NNLO) breaks down at low ϕ^* since the cross-section diverges due to emission of soft and co-linear gluons from initial state partons. Therefore, this prediction is not shown below $\phi^* = 0.3$. The resummation (RESBOS) [8] and parton shower (POWHEG+PYTHIA) [9][10] programmes do better at describing this region.

The results from the 2010 dataset for the Z and $W^\pm$ cross-sections and their ratios are shown in Figure 7. Luminosity uncertainties completely cancel in these ratios as well as some experimental systematics. For the theory predictions, PDF uncertainties partially cancel. The W^+ and W^- cross-sections are given below.

$$\sigma_{W^+ \to \mu^+\nu} = 831 \pm 9 \pm 27 \pm 29 \text{ pb}$$
$$\sigma_{W^- \to \mu^-\bar{\nu}} = 656 \pm 8 \pm 19 \pm 23 \text{ pb}$$

As can be seen from the plot, the W and Z cross-sections are in agreement with most PDF sets. There is some tension between the W^+ cross-section and the ABKM09 and NNPDF21 PDF sets. The lepton charge asymmetry $A_\mu = (\sigma_{W^+} - \sigma_{W^-})\,/\,(\sigma_{W^+} + \sigma_{W^-})$ (see [5]) and $\sigma_{W^+}/\sigma_{W^-} = 1.27 \pm 0.02 \pm 0.01$ ratio are sensitive to the ratio of the up and down valence quark PDFs. The $\sigma_{W^+}/\sigma_{W^-}$ ratio is measured here with a precision of about 1.7% which is comparable to the theoretical precision. As can be seen in the plot the ABKM09 set is slightly disfavoured by the data. The PDF uncertainty largely cancels in the ratio $(\sigma_{W^+} + \sigma_{W^-})\,/\sigma_Z = 19.4 \pm 0.5 \pm 0.9$. This is a precision test of the SM which we measure to about 5%.

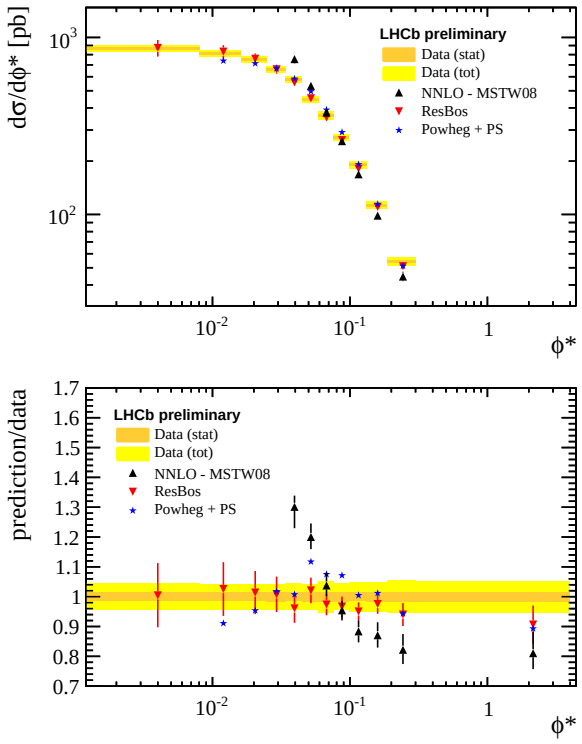

Figure 6. Top: Differential cross-sections for $Z \to \mu\mu$ as a function of ϕ^* using the 2011 dataset compared to predictions. The statistical and total errors on the data are shown as gold and yellow bands respectively. Predictions are shown as points. Bottom: Ratios of predictions to data for same.

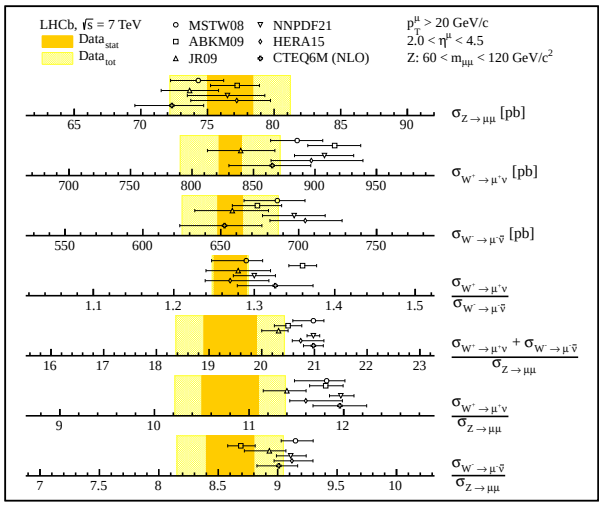

Figure 7. Cross-sections and ratios measured using the 2010 dataset. The statistical and total errors on the measurements are shown as gold and yellow bands respectively. The points are NNLO and NLO predictions with various PDF parameterisations.

5 Conclusions

Cross-sections and ratios of Z and W bosons have been measured in the muon channel on a dataset with an integrated luminosity of $37pb^{-1}$ collected during 2010 at a centre of mass energy of $\sqrt{s} = 7$ TeV. Cross-section ratios have also been measured. In the case of the $\sigma_{W^+}/\sigma_{W^-}$ ratio, the measurement is at a precision comparable to the theoretical precision. Z cross-sections in all leptonic channels have been measured using the $1fb^{-1}$ 2011 dataset. Measurements are consistent with NNLO predictions where they are known to be valid. At low ϕ^* better predictions for the Z cross-section are made by programmes which explicitly resum divergent terms or are interfaced with parton showers.

References

[1] LHCb Collaboration, JHEP **01** (2013) 111
[2] LHCb Collaboration, LHCb-CONF-2013-007
[3] LHCb Collaboration, JHEP **02** (2013) 106
[4] M.Vesterinen, T.R.Wyatt, Nucl.Instr.Meth. **602**, 432-437 (2009)
[5] LHCb Collaboration, JHEP **06** (2012) 058
[6] R.Gavin, Y.Li, F.Petriello, S.Quackenbush, Comput.Phys.Commun. **182** (2011) 2388
[7] A.D.Martin, W.J.Stirling, R.S.Thorne, G.Watt, Eur.Phys.J. **C63** (2009) 189
[8] G.A.Ladinsky, C.-P.Yuan, C.Balazs, F.Landry, R.Brock, Phys.Rev. **D50** (1994) 4239, Phys.Rev. **D56** (1997) 5558, Phys.Rev. **D67** (2003) 073016
[9] P.Nason, S.Frixione, C.Oleari, S.Alioli, JHEP **11** (2004) 040, JHEP **11** (2007) 070, JHEP **06** (2010) 043
[10] T.Sjöstrand, S.Mrenna, P.Skands, JHEP **05** (2006) 026